Quantum effects of solitons in the self-dual impurity model

I. Takyi[1] and H. Weigel[2]

[1]*Mathematics Department, Kwame Nkrumah University of Science and Technology, Private Mail Bag, University Post Office, KNUST-Kumasi, Ghana*

[2]*Institute for Theoretical Physics, Physics Department, Stellenbosch University, Matieland 7602, South Africa*

(Received 5 December 2022; accepted 13 January 2023; published 2 February 2023)

We compute the vacuum polarization energies (VPEs) of solitons in a self-dual impurity model in which the soliton profiles take the shape of a separated kink-antikink pair. Classically the soliton energies are invariant under the change of a continuous parameter that can be interpreted as the kink-antikink separation. This is not the case for the VPEs so that quantum effects decide on the energetically most favorable separation. The considered configurations are classically stable so that its quantum fluctuations have only real frequency eigenvalues. Hence, in contrast to the kink-antikink configuration in the ϕ^4 model, the VPE is well defined for any value of the separation and we gain insight into the quantum corrections to the kink-antikink potential.

DOI: 10.1103/PhysRevD.107.036003

I. INTRODUCTION

In this work we explore the one-loop quantum corrections to the energies of solitons in a self-dual impurity ϕ^4 model in one-space and one-time dimension ($D = 1 + 1$). Low-dimensional soliton models are interesting because they are role models for more complex systems in higher dimensions that have applications ranging from, among others, cosmology [1] via condensed matter physics [2,3] to hadron [4] and nuclear physics [5]. An important feature of the model that we consider here is that its solitons saturate a Bogomolny-Prasad-Sommerfield (BPS) [6,7] energy bound. Hence the classical energy only depends on the boundary values of soliton profiles but not on the position of the impurity so that there is no static force between the impurity and the soliton [8,9]. As a further consequence these solitons are degenerate with respect to the variation of a continuous parameter that measures the distance between the position of the kink-type structure and the center of the impurity. Thus the most favorable solution is determined by the quantum corrections to the classical energy even though these corrections are small for a consistent choice of model parameters. Computing these corrections as a function of this variational parameter is the central objective of this work. For a sufficiently strong impurity we will find a local minimum of the quantum energy. However, for weak impurities, this energy favors infinitely far separated kink-antikink pairs, signaling an unstable soliton. This is similar to multifield Shifman Voloshin soliton [10] that has classically degenerate solitons that are unstable quantum mechanically [11]. Similarly, quantum corrections reveal instabilities in higher polynomial soliton models [12,13].

For moderate and large values of the separation parameter the static solutions resemble superpositions of a kink-antikink pair in the renowned ϕ^4 model [14–16]. In contrast to kink-antikink superpositions in the ϕ^4 model the impurity causes such configurations to be stable classically so that the model provides a way around the fundamental problem of dealing with imaginary frequencies [17,18] of the quantum fluctuations about a kink-antikink in the ϕ^4 model.

The computation of quantum corrections to soliton energies in one space dimension is by now a standard and straightforward endeavor when utilizing the so-called spectral methods [19]. The essential ingredients are the scattering data extracted from the quantum fluctuations about the potential that is induced by the soliton. This computation is particularly simple when this potential is invariant under spatial reflection [20]. All that is needed is the Jost function along the positive imaginary momentum axis. Since the quantum energy manifests itself through the shift (or polarization) of the zero point energies of the quantum fluctuations it is frequently called the vacuum polarization energy (VPE).

Following this introduction, we will describe the self-dual impurity model and its BPS solutions in Sec. II. Section III contains the analysis of the potential for the quantum fluctuations at moderate and large kink-antikink separation. In Sec. IV we will describe the spectral method that determines the VPE. We will present the numerical

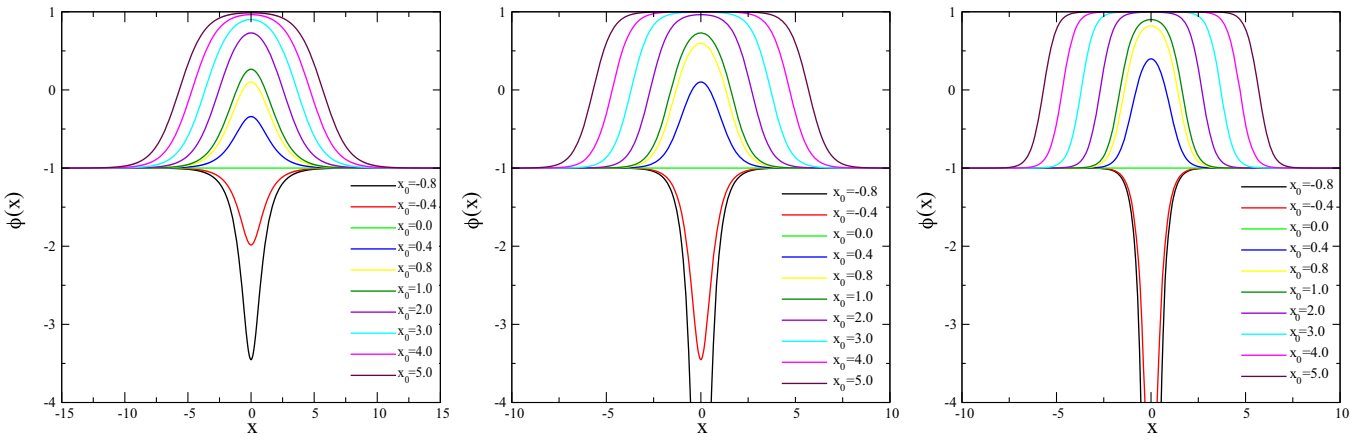

FIG. 1. From left to right: the profile of the BPS soliton in Eq. (5) for various values of the intersoliton distance (x_0) for $j = 1$, $j = 2$, and $j = 3$.

results for the VPE of BPS solutions in the self-dual impurity model in Sec. V. In Sec. VI we estimate the leading quantum correction to the kink-antikink potential. We conclude and summarize in Sec. VII.

II. THE MODEL

We consider the self-dual impurity model in $D = 1 + 1$ whose full Lagrangian is given by [21,22]

$$L = \int dx \left[\frac{1}{2}\left(\frac{\partial\phi}{\partial t}\right)^2 - \frac{1}{2}\left(\frac{\partial\phi}{\partial x} + \sqrt{2}W + \sqrt{2}\sigma W\right)^2\right] + \int dx\sqrt{2}W\frac{\partial\phi}{\partial x}, \tag{1}$$

where $W = W(\phi)$ is the superpotential and $\sigma = \sigma(x)$ is the prescribed impurity. In the limit $\sigma \to 0$ the standard scalar model with a scalar potential of $U = W^2$ is obtained. Typically these potentials generate spontaneous symmetry breaking with at least two degenerate vacua. The soliton(s) then assume either of them at positive and negative spatial infinity. We have written this Lagrangian in terms of dimensionless variables and parameters, thereby omitting an overall factor. This factor does not affect the field equations but, through canonical quantization, it is the order parameter that counts the loops entering the quantum corrections and thus discriminates between classical and quantum contributions. In our case we will solely compare configurations which are classically degenerate at one loop order. (Actually all configurations have zero classical energy.) Hence our results will not be sensitive to this order parameter and we may safely omit it.[1]

The topological lower bound of the classical energy is saturated when the following Bogomolny equation holds

$$\frac{\partial\phi}{\partial x} + \sqrt{2}W + \sqrt{2}\sigma W = 0. \tag{2}$$

In this study we take the superpotential to be

$$W = \frac{1}{\sqrt{2}}(1 - \phi^2), \tag{3}$$

which is of the ϕ^4 model type in the no impurity limit. In particular, we consider the nonlocalized impurity [21,22]

$$\sigma_j(x) = \frac{j}{2}\tanh(x) - 1, \tag{4}$$

where $j \geq 0$ is the parameter that measures the strength of the impurity. The BPS solutions in this self-dual impurity model are

$$\phi(x) = -\frac{\cosh^j x - a}{\cosh^j x + a}. \tag{5}$$

We may take either $a \in (-1, \infty)$ or

$$a = -1 + e^{jx_0} \quad \text{with} \quad x_0 \in \mathbb{R}, \tag{6}$$

as the variation parameter that parameterizes the shape of the BPS soliton profiles.

For $x_0 \gg 1$ the BPS solutions represent infinitely widely separated kink-antikink pairs of the ϕ^4 model as shown in Fig. 1. Also, as x_0 tends to 0, the kink and antikink approach each other. For small impurities with $0 < x_0 \lesssim 1$, a BPS solution is similar to a kink-antikink pair in the ϕ^4 model with small separation. However, for large impurities, the BPS solutions develop wells at the center. The variation parameter x_0 was interpreted as the distance between the BPS soliton and the impurity [22] because of these particular features.

[1]In general, this parameter should be chosen to make the leading quantum correction small; otherwise higher order effects will presumably be sizable.

In general BPS solutions saturate the topological energy bound and the static energy thus only depends on the boundary values of the soliton. In our case this has the important consequence that this energy is independent of the strength j of the impurity. Hence there is no (static) force between the BPS soliton and the impurity.

Obviously the superpotential vanishes at $\phi = \pm 1$ which are the two possible vacua. At spatial infinity the soliton approaches $\phi = -1$, which we thus call the primary vacuum. The equality between the profiles at positive and negative spatial infinity actually leads to a vanishing classical energy. Unless x_0 is very small, the soliton also occupies the secondary vacuum at $\phi = +1$ in a sizable region of space. This region grows with x_0. The possibility of occupying such a secondary vacuum has been recently related to quantum destabilization of solitons [11].

In the next step, we investigate the behavior of the scattering potential. We do this by considering a small perturbation of the BPS solitons $\phi(x,t) = \phi(x) + \eta(x)e^{-i\omega t}$. Substituting this into Eq. (1) and considering linear terms of η in the resulting wave equation yields

$$\left[-\frac{d^2}{dx^2} + V(x)\right]\eta = \omega^2\eta, \tag{7}$$

where $\omega^2 = m^2 + k^2$ with $k > 0$ for the scattering states and $k_j = i\kappa_j$ for the bound states. Here m and k are the mass of the fluctuations and the continuous momentum, respectively. Subtracting the analog quantity for $V(x \to \pm\infty) = m^2$ from the wave equation yields the scattering wave equation

$$\left[-\frac{d^2}{dx^2} + u(x)\right]\eta = k^2\eta, \tag{8}$$

where

$$\begin{aligned} u(x) &= V(x) - m^2 \\ &= 2(1+\sigma)^2\left[\left(\frac{dW}{d\phi}\right)^2 + W\frac{d^2W}{d\phi^2}\right] \\ &\quad - \sqrt{2}\frac{\partial\sigma}{\partial x}\frac{dW}{d\phi} - m^2 \end{aligned} \tag{9}$$

is the scattering potential. We also identify $m = j$ from $u(x) \to 0$ when $x \to \infty$. The explicit expression for the scattering potential is obtained by substituting the BPS soliton $\phi(x)$, the nonlocalized impurity $\sigma_j(x)$, and the superpotential $W(\phi(x))$. This then takes the form

$$\begin{aligned} u(x) = \frac{j^2}{2}&\left[\left(3\left[\frac{\cosh^j x - a}{\cosh^j x + a}\right]^2 - 1\right)\tanh^2 x - 2\right] \\ &- \frac{j}{\cosh^2 x}\frac{\cosh^j x - a}{\cosh^j x + a}. \end{aligned} \tag{10}$$

The shape of the scattering potential is shown in Fig. 2. We observe that for small j the potential has two noncentral attractive regions in the vicinity of $\pm x_0$. As we increase j a central structure around the origin emerges that is fully attractive for large j. For small and moderate j it has both attractive and repulsive components.

Since the classical energy does not depend on x_0, we expect a zero mode whose wave function is proportional to

$$\eta_0(x) = \frac{\partial\phi(x)}{\partial x_0} \propto \frac{\partial\phi(x)}{\partial a} = \frac{2\cosh^j x}{(\cosh^j x + a)^2}. \tag{11}$$

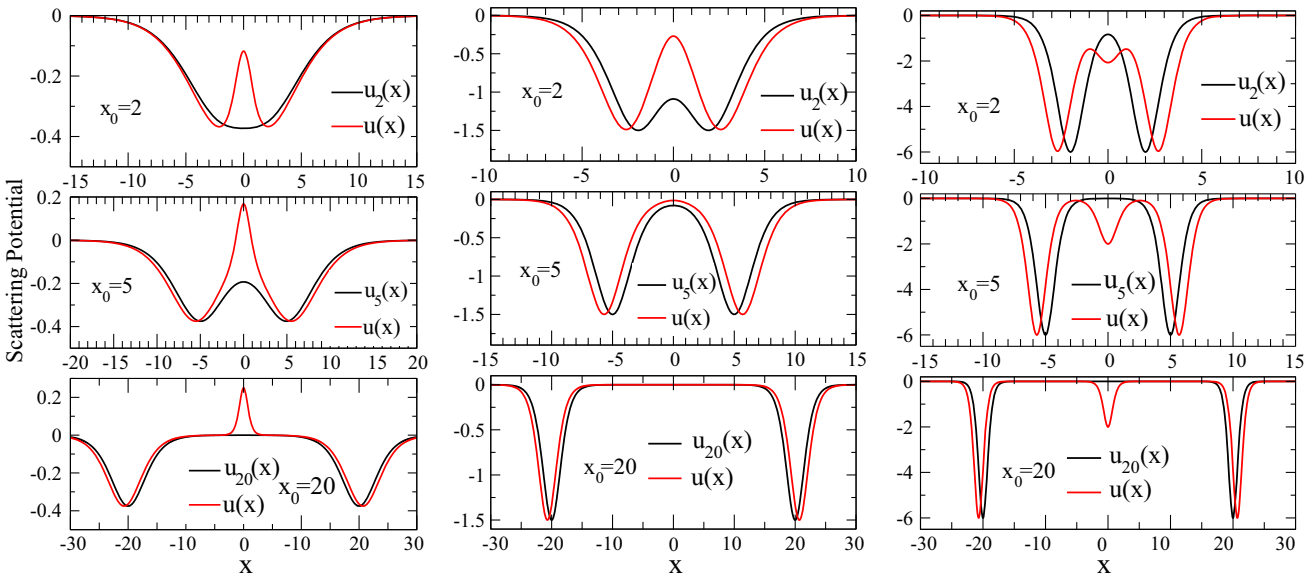

FIG. 2. The scattering potential $u(x)$ from Eq. (10) compared to that of the ϕ^4 configuration $u_{x_0}(x)$ for $x_0 = 2$, 5, and 20. The latter is defined in Eq. (24). Left to right: for $j = 0.5$, 1, and 2. Note the different scales along the horizontal axis as x_0 varies.

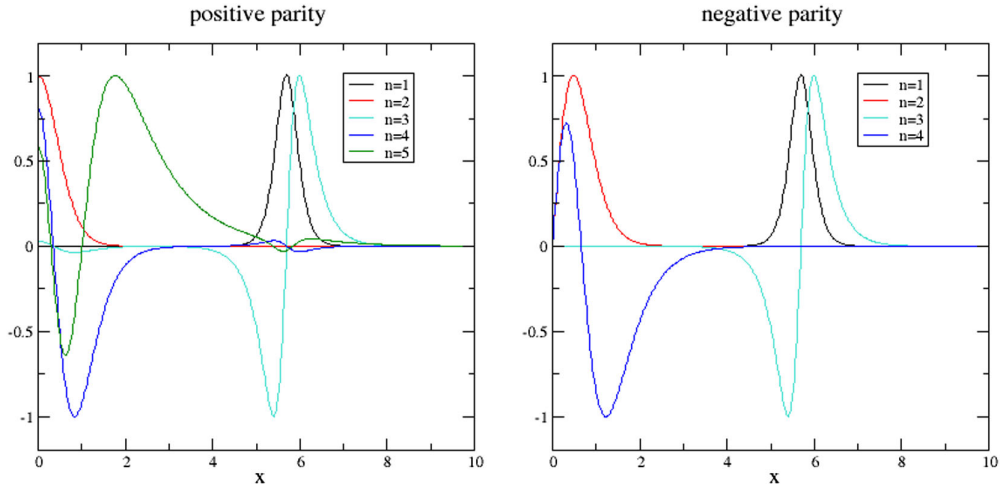

FIG. 3. Bound state wave functions for $x_0 = 5.0$ and $j = 6.0$. The solutions labeled $n = 1$ are the asymptotic ($x_0 \to \infty$) zero modes. We have normalized the wave functions to be in the interval $[-1, 1]$.

III. SCATTERING POTENTIAL AT LARGE x_0

We want to investigate the potential for large $a \approx e^{jx_0}$ in the three regimes where it substantially deviates from zero: (i) $x \approx x_0$, (ii) $x \approx -x_0$, and (iii) $x \approx 0$. The first two are equivalent by spatial reflection.

For (i) and (ii) we can set $\tanh^2 x = 1$. To be definite we consider (i) so that $\cosh^j x \approx \frac{1}{2^j} e^{jx} = e^{j(x-\ln 2)}$. We then have

$$\frac{\cosh^j x - a}{\cosh^j x + a} \approx \frac{e^{j(x-\ln 2)} - e^{jx_0}}{e^{j(x-\ln 2)} - e^{jx_0}} = \frac{e^{j(x-x_0-\ln 2)} - 1}{e^{j(x-x_0-\ln 2)} + 1} = \tanh\left[\frac{j}{2}(x - x_0 - \ln 2)\right]. \quad (12)$$

This approximates the potential as

$$u(x) \approx \frac{3}{2} j^2 \left\{ \tanh^2\left[\frac{j}{2}(x - x_0 - \ln 2)\right] - 1 \right\}, \quad (13)$$

which is a Pöschl-Teller potential[2] with $M = j$ and $l = 2$ centered at $x_0 + \ln 2$. Its bound state energies have wave numbers $t = \sqrt{j^2 - \epsilon^2}$ with $t = \frac{j}{2}$ and $t = j$. This approximation also shows that the zero mode associated with the x_0 invariance of the classical energy turns into the translational zero mode of an ordinary kink. By a similar analysis we get

$$\phi(x) = -\frac{\cosh^j(x) - a}{\cosh^j(x) + a} \approx -\tanh\left[\frac{j}{2}(x - x_0 - \ln 2)\right] \quad (14)$$

for large a and $x \approx x_0$, which again exhibits the antikink structure located at $x_0 + \ln 2$. With the kink potential $\frac{\lambda}{4}(\phi^2 - \frac{M^2}{2\lambda})^2$ this corresponds to $M = j$ and $\lambda = \frac{j^2}{2}$. Along the same considerations we find a kink structure around $-(x_0 + \ln 2)$.

For case (iii) we have $a \gg \cosh^j x$ and thus

$$u(x) \approx j(j-1)[\tanh^2(x) - 1]. \quad (15)$$

The bound state wave numbers of this potential are also known[3]

$$t = j - n - 1 \quad \text{with} \quad n = 0, 1, \ldots, \lfloor j \rfloor - 1. \quad (16)$$

The numerical simulation verifies these solutions for large j and x_0; including the zero mode wave functions being centered at $x_0 + \ln 2$ as can be seen from the numerical results shown in Fig. 3. Since $u(-x) = u(x)$, the bound states have definite parity.

In the process of these numerical simulations we have also verified the existence of the zero mode with the wave function, Eq. (11) for various values of j and x_0.

For $j = 1$ and large a the central part of the potential (iii) vanishes. Hence we expect that in this case the VPE is (twice) that of the kink with $M = 1$.

IV. VACUUM POLARIZATION ENERGY

The VPE is a measure of the energy change caused by the polarization of the single particle modes, which occurs due to the interaction of quantum fluctuations with the background configuration generated by the soliton. As already discussed the soliton induces a reflection invariant potential and we can therefore write the renormalized boson VPE as

[2]These potentials are $V_l = \frac{l+1}{l} M^2[\tanh^2(Mx/l) - 1]$. The bound state wave numbers are $t = \sqrt{M^2 - E^2} = kM/l$ with $k = 0, 1, 2, \ldots, l$.

[3]See, e.g., Eqs. (3.11) and (3.12) in Ref. [23].

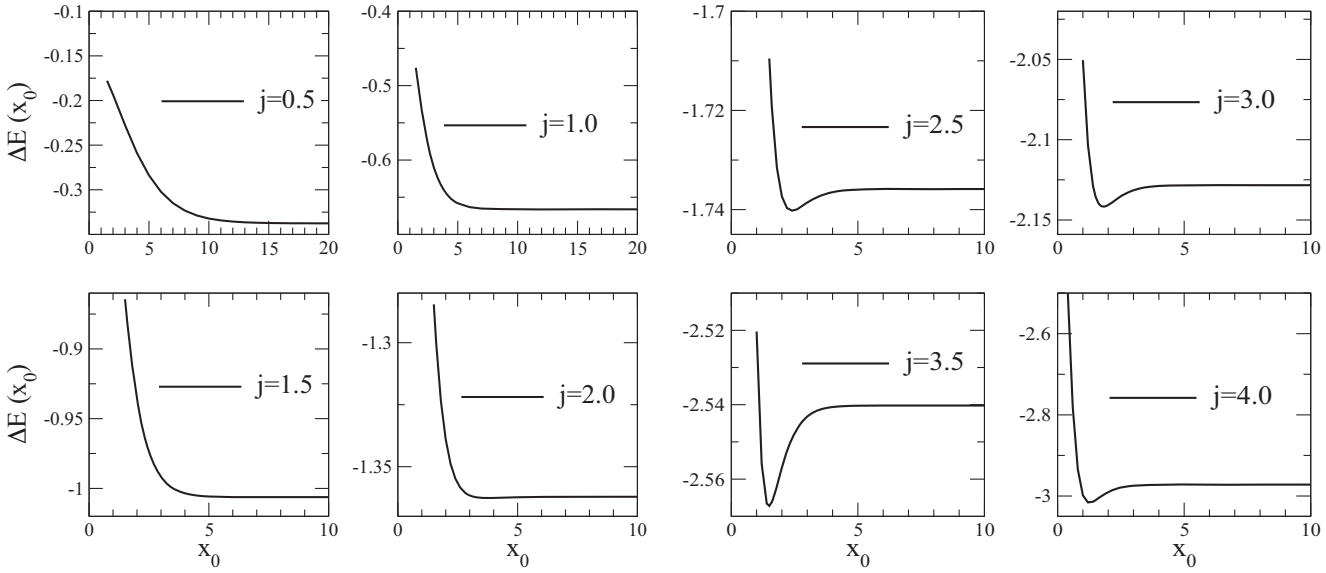

FIG. 4. The vacuum polarization energy as a function of x_0 for various values of j. Note the different horizontal scales for small j.

$$\Delta E = \frac{1}{2}\sum_{n}^{\text{b.s.}} \omega_n + \int_0^\infty \frac{dk}{2\pi} \sum_{\ell=\pm} \sqrt{k^2+j^2}\left[\frac{d\delta_\ell(k)}{dk}\right]_N + \sum_{n=1}^{N} E_{\text{FD}}^{(n)} + E_{\text{CT}}. \tag{17}$$

The first term sums over the explicit bound states and the momentum integral (with the sum over the parity channels) collects the continuum contribution. It is the integral over the scattering states with the relativistic dispersion $\omega = \sqrt{k^2+j^2}$ weighted by the change in the density of states expressed by the phase shift according to the Krein formula [24],

$$\Delta\rho_\ell = \frac{1}{\pi}\frac{d\delta_\ell(k)}{dk}. \tag{18}$$

The subscript N indicates the subtraction of the first N orders of the Born series from the phase shifts. With N sufficiently large, the momentum integral is finite. These subtractions are added back in the form of equivalent Feynman diagram contributions, $E_{\text{FD}}^{(n)}$. Finally, E_{CT} is the counterterm contribution that implements the renormalization condition(s). Note that $\sum_{n=1}^{N} E_{\text{FD}}^{(n)} + E_{\text{CT}}$ is also ultraviolet finite. For a boson fluctuation in one space dimension the situation is quite simple. There is only one ultraviolet divergent Feynman diagram with a single insertion of the (Fourier transform at zero momentum of) $u(x)$. It is proportional to $\int_0^\infty dx\, u(x)$ and can thus be canceled completely within the so-called no-tadpole renormalization scheme. Hence we write

$$\Delta E = \frac{1}{2}\sum_{n}^{\text{b.s.}} \omega_n + \int_0^\infty \frac{dk}{2\pi} \sum_{\ell=\pm} \sqrt{k^2+j^2}\left[\frac{d\delta_\ell(k)}{dk}\right]_1. \tag{19}$$

The phase shifts are the phases of the Jost functions $F_+(k) = \lim_{x\to 0} \frac{\partial \mathcal{F}(k,x)}{ik\partial x}$ and $F_-(k) = \lim_{x\to 0}\mathcal{F}(k,x)$ in the two parity channels. Here $\mathcal{F}(k,x)$ solves the wave equation, Eq. (8), with the boundary condition $\lim_{x\to\infty} e^{-ikx}\mathcal{F}(k,x) = 1$. This function is the Jost solution and is analytic for $\mathrm{Im}(k) \geq 0$ [25,26]. For real k we also have $\mathcal{F}(-k,x) = \mathcal{F}^*(k,x)$ so that we express the phase shifts as an obviously odd function of the momentum: $\delta_\ell(k) = \frac{i}{2}[\ln F_\ell(k) - \ln F_\ell(-k)]$. In turn we get the VPE

$$\Delta E = \frac{1}{2}\sum_{n}^{\text{b.s.}} \omega_n + \frac{i}{2}\int_{-\infty}^{\infty} \frac{dk}{2\pi}\sqrt{k^2+j^2}\left[\frac{d\ln F_+(k)F_-(k)}{dk}\right]_1. \tag{20}$$

This integral can be computed as a contour integral because $F_\pm(k)$ is analytic in the upper complex momentum plane. As the leading large $|k|$ terms are Born subtracted there is no contribution from the semicircle at infinity. The Jost function has simple zeros at the complex bound state momenta $k = i\sqrt{j^2-\omega_n^2}$ so that the singularities from the logarithmic derivative cancel $\frac{1}{2}\sum_n^{\text{b.s.}} \omega_n$. The only contribution stems from bypassing the branch cut induced by the relativistic dispersion relation along the imaginary axis $t \in [j,\infty]$, where $k = it$. To efficiently compute that final integral we factorize $\mathcal{F}(it,x) = e^{-tx} g(t,x)$ and solve the differential equation

$$\frac{\partial^2 g(t,x)}{\partial x^2} = 2t\frac{\partial g(t,x)}{\partial x} + u(x)g(t,x), \tag{21}$$

with boundary condition $g(t,\infty)=1$. After a final integration by parts we get

$$\Delta E=\int_j^\infty \frac{dt}{2\pi}\frac{t}{\sqrt{t^2-j^2}}\left\{\ln\left[g(t,0)\left(g(t,0)-\frac{1}{t}\frac{\partial g(t,x)}{\partial x}\bigg|_{x=0}\right)\right]-\frac{1}{t}\int_0^\infty dx\,u(x)\right\}. \tag{22}$$

We have made the Born subtraction explicit. The coefficient of that spatial integral can be most straightforwardly derived by expanding $g(t,x)=1+g^{(1)}(t,x)+\mathcal{O}(u^2)$ and integrating the corresponding differential equation

$$\frac{\partial^2 g^{(1)}(t,x)}{\partial x^2}=2t\frac{\partial g^{(1)}(t,x)}{\partial x}+u(x),$$

with the boundary condition $g^{(1)}(t,\infty)=0$ along the positive half axis in coordinate space.

V. NUMERICAL RESULTS FOR THE VPE

In this section, we report the results from our numerical simulations of the one-loop VPE discussed above. We solve Eq. (21) using the fourth order Runge-Kutta algorithm with an adaptive step size control for various values of j and x_0. That is, we compute the quantum correction to the energy as a function of the variational parameter, x_0 with respect to which the classical energy is degenerate.

As indicated earlier, the BPS solution behaves like a superposition of the kink-antikink configuration in the ϕ^4 model approximated by

$$\phi_R(x)=\tanh\left[\frac{j}{2}(x+R)\right]-\tanh\left[\frac{j}{2}(x-R)\right]-1, \tag{23}$$

where R indicates the position of the kink. This configuration gives rise to the scattering potential

$$u_R(x)=\frac{3j^2}{2}[\phi_R^2(x)-1]. \tag{24}$$

In Fig. 2 we also compare this to the BPS scattering potential. We see that $j=1$ best approximates the kink-antikink configuration of the ϕ^4 model for $x_0\gg 1$. This confirms the approximation, Eq. (15) according to which the central structure vanishes for this value of j when x_0 is large. The only difference is that the position of the potential minimum is somewhat larger than R; of course this is just the additional ln 2 identified in Sec. III. For $j\gtrsim 5$ the noncentral structures of $u(x)$ almost exactly match $u_R(x)$, with the same small deviation of the minimum position from R.

We display the results for ΔE as a function of x_0 from our numerical simulations for other impurity values in Tables I–V, each referring to different values of j. We observe that ΔE decreases when increasing x_0 from a small finite value to infinity. For small j it does so monotonously but develops a tiny local minimum at a moderate x_0 when j increases. This is due to the attractive central structure of $u(x)$. The position of the local minimum moves to smaller values of x_0 as j increases. This is also obvious from the graphs in Fig. 4. Hence we conclude that for a significantly strong impurity the quantum corrections resolve the classical degeneracy while for weak impurities $x_0\to\infty$ is favored, which causes the soliton to be unstable. From Fig. 4 and Table IV we immediately recognize an energy minimum for $j=2$. For $j=1.5$ the existence of such a

TABLE I. VPE as function of x_0 for $j=0.2$.

x_0	1.5	4.0	8.0	12.0	16.0	20.0	24.0	28.0	32.0	36.0	40.0	44.0
ΔE	−0.06455	−0.06992	−0.09204	−0.11242	−0.12575	−0.13312	−0.13681	−0.13856	−0.13937	−0.13974	−0.13990	−0.13995

TABLE II. Behavior of the VPE as function of x_0 for $j=0.5$.

x_0	1.5	2.0	3.0	4.0	5.0	6.0	7.0	8.0	9.0	10.0
ΔE	−0.17786	−0.19343	−0.22755	−0.25882	−0.28383	−0.30221	−0.31493	−0.32336	−0.32878	−0.33219
x_0	11.0	12.0	13.0	14.0	15.0	16.0	17.0	18.0	19.0	20.0
ΔE	−0.33431	−0.33562	−0.33642	−0.33691	−0.33721	−0.33739	−0.33749	−0.33754	−0.33756	−0.33758

TABLE III. VPE as function of x_0 for $j=1.0$, whose asymptotic value is twice the VPE value of a single kink of the ϕ^4 model.

x_0	1.5	2.0	3.0	4.0	5.0	6.0	7.0	8.0	9.0	10.0
ΔE	−0.475999	−0.53358	−0.60935	−0.64415	−0.65805	−0.66328	−0.66523	−0.66599	−0.66617	−0.66622
x_0	11.0	12.0	13.0	14.0	15.0	16.0	17.0	18.0	19.0	20.0
ΔE	−0.66623	−0.66623	−0.66623	−0.66623	−0.66623	−0.66623	−0.66623	−0.66623	−0.66623	−0.66623

TABLE IV. VPE as function of x_0 for $j = 2.0$.

x_0	1.5	2.0	3.0	4.0	5.0	6.0	7.0	8.0	9.0
ΔE	−1.28454	−1.33903	−1.36159	−1.36259	−1.36230	−1.36217	−1.36214	−1.36213	−1.36213
x_0	10.0	11.0	12.0	13.0	14.0	15.0	16.0	17.0	18.0
ΔE	−1.36213	−1.36213	−1.36213	−1.36213	−1.36213	−1.36213	−1.36213	−1.36213	−1.36213

TABLE V. VPE as function of x_0 for $j = 2.5$.

x_0	1.5	2.0	3.0	4.0	5.0	6.0	7.0	8.0	9.0
ΔE	−1.70952	−1.73737	−1.73857	−1.73648	−1.73594	−1.73586	−1.73585	−1.73585	−1.73585
x_0	10.0	11.0	12.0	13.0	14.0	15.0	16.0	17.0	18.0
ΔE	−1.73585	−1.73585	−1.73585	−1.73585	−1.73585	−1.73585	−1.73585	−1.73585	−1.73585

very shallow minimum is not obvious from the figure. However, the data $\Delta E(7.0) - \Delta E(15.0) = -0.0004$ indeed indicate the existence of a minimum already for $j = 1.5$. Even though this small difference is of the order of the numerical accuracy we conjecture that minima emerge for all $j > 1$ since for this value and large enough x_0 the central structure of $u(x)$ turns from repulsive to attractive at $j = 1$; as discussed in Sec. III. Eventually the VPE saturates when x_0 is large enough because the various structures in $u(x)$ separate without changing their shapes as x_0 grows further. For weak impurities the asymptotic value is (approximately) reached only for very large x_0 but the saturation position decreases as j increases. Again, this can be understood from the discussion in Sec. III: the larger j, the better the approximation $\cosh^j(x - x_0) \approx e^{j(x-x_0-\ln 2)}$.

With increasing impurity strength the local minimum in ΔE moves to smaller x_0 values and the x_0 behavior of the soliton profile shown in Fig. 1 suggests that the soliton eventually loses its kink-antikink shape.

The case $j = 1$ is particularly interesting because we have conjectured that the central structure becomes irrelevant as x_0 increases and that the potential in the vicinity of $\pm x_0$ is of Pöschl-Teller type with $l = 2$. That is exactly the background potential induced by the kink in a ϕ^4 model. And indeed we see from Table III that ΔE approaches −0.66623 asymptotically which is twice the Dashen-Hasslacher-Neveu [27] value $(\frac{1}{4\sqrt{3}} - \frac{3}{2\pi}) \approx -0.333127$ for the VPE of the ϕ^4 kink soliton for unit mass parameter. Though supported by the analytical considerations in Sec. III in the limit of large x_0, this agreement occurs already for moderate x_0. For example, for $x_0 = 5$ the difference in the VPEs is just about 1%.

VI. QUANTUM CORRECTIONS TO THE KINK-ANTIKINK POTENTIAL

We identify the scattering potential associated with the central region by defining

$$\tilde{u}(x) = u(x)\begin{cases} 1 & |x| \le \frac{x_0}{2} \\ e^{-(|x|-x_0/2)^2/w^2} & |x| > \frac{x_0}{2} \end{cases}, \tag{25}$$

TABLE VI. The quantum correction to the kink-antikink potential, Eq. (26) as a function of x_0 for $j = 0.5$ and $w = 2.0$.

x_0	1.0	3.0	5.0	7.0	9.0	11.0	13.0
$\Delta E_{K\bar{K}}$	−0.1448	−0.2182	−0.2766	−0.3088	−0.3235	−0.3295	−0.3317

TABLE VII. Same as Table VI for $j = 2.5$.

x_0	1.0	2.0	3.0	4.0	5.0	6.0	7.0
$\Delta E_{K\bar{K}}$	−1.4350	−1.6505	−1.6657	−1.6659	−1.6657	−1.6656	−1.6656

TABLE VIII. Same as Table VI for $j = 4.0$.

x_0	1.0	2.0	3.0	4.0	5.0	6.0	7.0
$\Delta E_{K\bar{K}}$	−2.6254	−2.6836	−2.6684	−2.6655	−2.6651	−2.6650	−2.6650

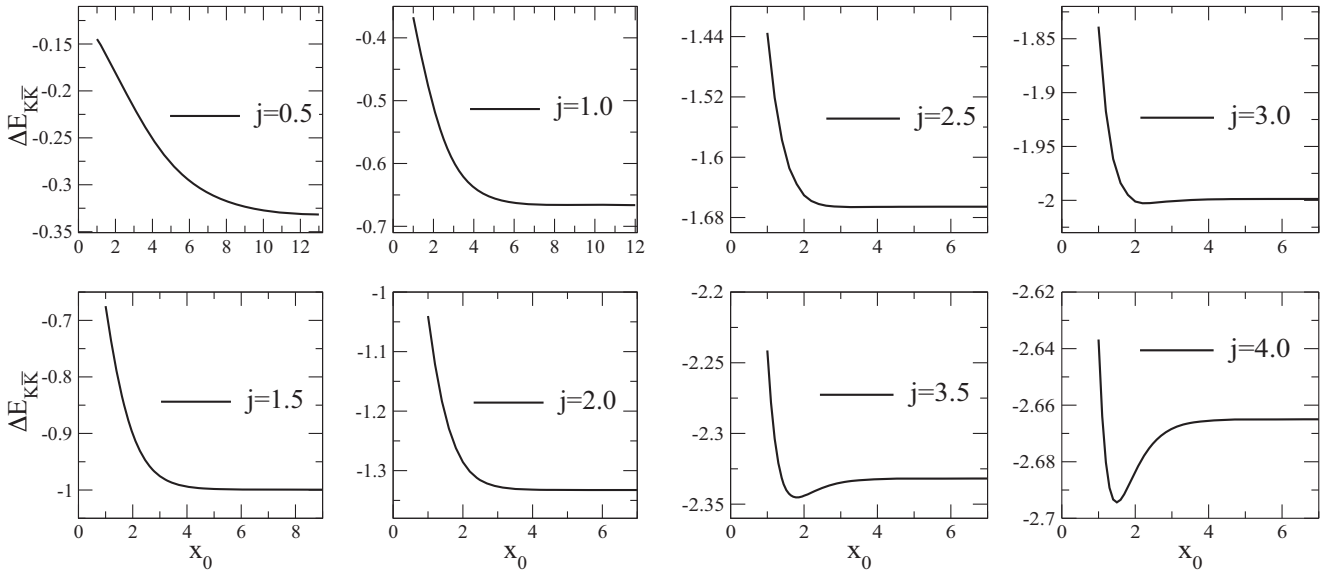

FIG. 5. The quantum correction to the kink-antikink potential, Eq. (26) as a function of x_0 and various values of j.

and we compute the corresponding VPE, $\widetilde{\Delta E}$. For large enough x_0 this is not sensitive to the width parameter w as long as it still small compared to x_0. The quantum correction to the kink-antikink potential is the difference

$$\Delta E_{K\bar{K}} = \Delta E - \widetilde{\Delta E}. \tag{26}$$

A direct identification of this correction would lead to imaginary frequencies (equivalently, zeros of the Jost function for $t > j$) for the would-be zero mode(s) because the static configuration from Eq. (23) is not a solution to the kink wave equation. In a sense we can interpret the central structure as the source needed to keep the ϕ^4 (anti)kink in place [28].

The numerical results for $\Delta E_{K\bar{K}}$ as functions of x_0 for different strengths j of the impurity are shown in Tables VI–VIII and Fig. 5. In all cases we reproduce the expected asymptotic value $\Delta E_{K\bar{K}} \to j(\frac{1}{2\sqrt{3}} - \frac{3}{\pi})$ for $x_0 \to \infty$ suggested via the Pöschl-Teller potential in Eq. (13).

As in the case of ΔE, $\Delta E_{K\bar{K}}$ is purely repulsive for small and moderate j. However, for $j \gtrsim 2$ a local minimum emerges. The x_0 position of this minimum approaches the center as j increases. We therefore conclude that the attraction for larger j is not only a property of the central structure of the fluctuation potential but also signals an attractive quantum contribution to the kink-antikink interaction. The energies shown in Fig. 5 suggest that the interaction becomes arbitrarily strongly repulsive as x_0 approaches zero. Thus would eventually prevent the kink-antikink system from collapsing (as it may in the pure ϕ^4 model). Unfortunately, extracting this interaction via Eq. (26) becomes an invalid procedure in that interesting limit.

VII. CONCLUSION

We have computed the leading (one-loop) quantum correction to soliton energies in an BPS-impurity model in one time and one space dimensions. Our motivation for this study was twofold. First, with the model parameters set to the BPS case, the classical energy is degenerate with respect to a continuous real parameter. Usually one trusts the computation of the leading quantum correction only when it is (significantly) smaller than the classical counterparts; otherwise it is very likely that even higher order corrections are equally important and should not be omitted. (See, e.g., Ref. [29] for estimates beyond one loop.) However, when comparing classically degenerate configurations, the classical energy is irrelevant and the quantum corrections are decisive for selecting the favorable configuration. Second, the above mentioned continuous parameter can be associated with the separation of a kink-antikink pair in the renowned ϕ^4 kink model, at least for moderate and large values. This allows us to investigate the quantum corrections to the kink-antikink interaction, which, due the emergence of unstable fluctuation modes, is unfortunately not directly possible in the ϕ^4 kink model.

In this model the soliton solution generates a potential for the quantum fluctuations with three structures. We have identified these structure from analytic considerations and also by exploring the bound state structure. Two of these structures can be associated with the kink and the antikink at the respective positions while the impurity induces a central structure in between. For small strengths of the impurity the central structure is repulsive but gets more and more attractive as this strength is increased. As consequences, for weak impurities the quantum fluctuations destabilize the soliton in the sense that it is energetically favorable to pull the kink and the antikink components

infinitely far apart. This means that the soliton occupies a secondary vacuum in an ever increasing region of space. Hence this instability is conceptually similar to the one previously observed in the Shifman-Voloshin model. As the strength increases the potential extracted from the quantum fluctuations develops a minimum that determines the favorable value of the parameter with respect to which the classical energy is degenerate. The more the impurity strength is increased the more the soliton loses its kink-antikink shape.

When we remove the central structure from the potential, we can get some insight into the quantum corrections to the kink-antikink interaction in the ϕ^4 model. Unfortunately, the corresponding results depend on the impurity strength so that we cannot make a general statement. However, we find that these corrections are mostly repulsive, only for large strengths a moderate attraction occurs.

We note that the choice for the impurity is somewhat arbitrary. The choice considered in Ref. [30] generates an antikink. Similar to the present case, the classical energy is not dependent on the distance between the centers of the antikink and the impurity. Using the technique[4] of Ref. [31], those authors hence computed the quantum correction to the energy as a function of that distance but did not observe a local minimum. It would be interesting to verify that result using the spectral method approach. Eventually the comparison of the VPEs for various impurities can further disentangle the effects stemming from the soliton on one side and the impurity on the other.

ACKNOWLEDGMENTS

H. W. is supported in part by the National Research Foundation of South Africa (NRF) by Grant No. 109497. The authors thank C. Halcrow for bringing Ref. [30] to their attention.

[4]That technique relates the creation and annihilation operators for the quantum fluctuations with and without a soliton background. For the standard kink, Ref. [31] reproduced the well-established historic result [27] and thus agrees with the spectral method [19].

[1] A. Vilenkin and E. P. S. Shellard, *Cosmic Strings and Other Topological Defects* (Cambridge University Press, Cambridge, England, 2000).
[2] U. Schollwöck *et al.*, *Quantum Magnetism*, Lecture Notes in Physics (Springer, New York, 2004), Vol. 645.
[3] N. Nagaosa and Y. Tokura, Nat. Nanotechnol. **8**, 899 (2013).
[4] H. Weigel, *Chiral Soliton Models for Baryons*, Lecture Notes in Physics (Springer, New York, 2008), Vol. 743.
[5] D. T. J. Feist, P. H. C. Lau, and N. S. Manton, Phys. Rev. D **87**, 085034 (2013).
[6] E. B. Bogomolny, Sov. J. Nucl. Phys. **24**, 449 (1976).
[7] M. K. Prasad and C. M. Sommerfield, Phys. Rev. Lett. **35**, 760 (1975).
[8] C. Adam and A. Wereszczynski, Phys. Rev. D **98**, 116001 (2018).
[9] C. Adam, T. Romanczukiewicz, and A. Wereszczynski, J. High Energy Phys. 03 (**2019**) 131.
[10] M. A. Shifman and M. B. Voloshin, Phys. Rev. D **57**, 2590 (1998).
[11] H. Weigel and N. Graham, Phys. Lett. B **783**, 434 (2018).
[12] H. Weigel, Phys. Lett. B **766**, 65 (2017).
[13] I. Takyi, M. K. Matfunjwa, and H. Weigel, Phys. Rev. D **102**, 116004 (2020).
[14] D. K. Campbell, J. F. Schonfeld, and C. A. Wingate, Physica (Amsterdam) **9D**, 1 (1983).
[15] P. Anninos, S. Oliveira, and R. A. Matzner, Phys. Rev. D **44**, 1147 (1991).
[16] I. Takyi and H. Weigel, Phys. Rev. D **94**, 085008 (2016).
[17] N. Graham and R. L. Jaffe, Phys. Lett. B **435**, 145 (1998).
[18] Z. Lee and H. Weigel, in *61st Annual Conference of the South African Institute of Physics* (SAIP, Pretoria, 2015), p. 512.
[19] N. Graham, M. Quandt, and H. Weigel, *Spectral Methods in Quantum Field Theory* (Springer, New York, 2009), Vol. 777.
[20] N. Graham and H. Weigel, Int. J. Mod. Phys. A **37**, 2241004 (2022).
[21] C. Adam, K. Oles, J. M. Queiruga, T. Romanczukiewicz, and A. Wereszczynski, J. High Energy Phys. 07 (2019) 150.
[22] C. Adam, K. Oles, T. Romanczukiewicz, and A. Wereszczynski, Phys. Rev. D **101**, 105021 (2020).
[23] V. A. Gani, M. A. Lizunova, and R. V. Radomskiy, J. High Energy Phys. 04 (2016) 043.
[24] J. S. Faulkner, J. Phys. C **10**, 4661 (1977).
[25] R. G. Newton, *Scattering Theory of Waves and Particles* (Springer, New York, 1982).
[26] K. Chadan and P. C. Sabatier, *Inverse Problems in Quantum Scattering Theory* (Springer, New York, 1989).
[27] R. F. Dashen, B. Hasslacher, and A. Neveu, Phys. Rev. D **10**, 4114 (1974).
[28] S. V. Bashinsky, Phys. Rev. D **61**, 105003 (2000).
[29] J. Evslin, Phys. Lett. B **822**, 136628 (2021).
[30] J. Evslin, C. Halcrow, T. Romanczukiewicz, and A. Wereszczynski, Phys. Rev. D **105**, 125002 (2022).
[31] J. Evslin, J. High Energy Phys. 11 (2019) 161.